Available online at www.sciencedirect.com
SCIENCE DIRECT®
Journal of Catalysis 224 (2004) 206–217
JOURNAL OF CATALYSIS
www.elsevier.com/locate/jcat

The Brønsted–Evans–Polanyi relation and the volcano curve in heterogeneous catalysis

T. Bligaard,[a] J.K. Nørskov,[a,*] S. Dahl,[b] J. Matthiesen,[b] C.H. Christensen,[a,b,c] and J. Sehested[b]

[a] *Center for Atomic-Scale Materials Physics, Department of Physics, Technical University of Denmark, Building 307, DK-2800 Lyngby, Denmark*
[b] *Haldor Topsøe A/S, Nymøllevej 55, DK-2800 Lyngby, Denmark*
[c] *Interdisciplinary Research Center for Catalysis, Department of Chemistry, Technical University of Denmark, Building 206, DK-2800 Lyngby, Denmark*

Received 30 October 2003; revised 24 February 2004; accepted 24 February 2004

Abstract

A number of elementary reactions at metal surfaces show a linear Brønsted–Evans–Polanyi relation between the activation energy and the reaction energy, and reactions belonging to the same class even follow the same relation. We investigate the implications of this finding on the kinetics of surface-catalyzed chemical processes. We focus in particular on the variation in the activity from one metal to the next. By analyzing a number of simple microkinetic models we show that the reaction rate under given reaction conditions shows a maximum as a function of the dissociative adsorption energy of the key reactant, and that for most conditions this maximum is in the same range of reaction energies. We also provide a database of chemisorption energies calculated using density-functional theory for a number of simple gas molecules on 13 different transition metals. An important part of the analysis consists of developing a general framework for analyzing the maximum rate. We use these concepts to rationalize trends in the catalytic activity of a number of metals for the methanation process.

Keywords: Linear free energy relationships; Microkinetic models; Density Functional Theory; Periodic trends in catalysis; Bond energies; Methanation

1. Introduction

One of the most fundamental concepts in heterogeneous catalysis is the volcano curve [1]. It has been established empirically that a volcano-shaped curve is obtained when the activity of catalysts for a certain reaction is plotted as a function of a parameter relating to the ability of the catalyst surface to form chemical bonds to reactants, reaction intermediates, or products [2,3]. Such relations are interesting from a scientific point of view since they point to important aspects of the reaction, and they are also useful as guidelines in the search for new catalysts [4,5].

An important problem in connection with volcano curves is which fundamental parameters the catalytic activity depends on. Activities have been correlated with various electronic properties of the catalyst [1], and it seems natural to relate the activity to bond energies. Here bond energies derived from bulk carbide or oxide properties [5,6] or various atomic or molecular chemisorption energies [7] have been used. The question is which energy is the most relevant. In addition there is a problem of finding systematic databases of relevant surface thermo-chemical data. The fact that many volcano curves are plotted as a function of a bulk heat of formation is related to the latter problem—only bulk thermochemical data are widely available. In the present paper we will address both problems. We will discuss in some detail the choice of the most relevant interaction energy that describes the catalytic activity of a metal surface, and we will present extensive surface thermo-chemical databases based on density-functional theory calculations.

It was recently established that for dissociative chemisorption of a number of molecules the activation energy depends linearly on the reaction energy[1] [8–11]. Such a Brønsted–Evans–Polanyi (BEP) relation has often been assumed implicitly to hold for surface reactions, and in a few cases a BEP relation has been established for a set of catalysts [6]. It is, however, only with the extensive use of

* Corresponding author. Fax: +45 4593 2399.
E-mail address: norskov@fysik.dtu.dk (J.K. Nørskov).

[1] Throughout the paper all reaction energies, ΔE (e.g., adsorption energies), are given with the same sign convention as reaction enthalpies. This means that an exothermic reaction has negative reaction energy.

0021-9517/$ – see front matter
doi:10.1016/j.jcat.2004.02.034

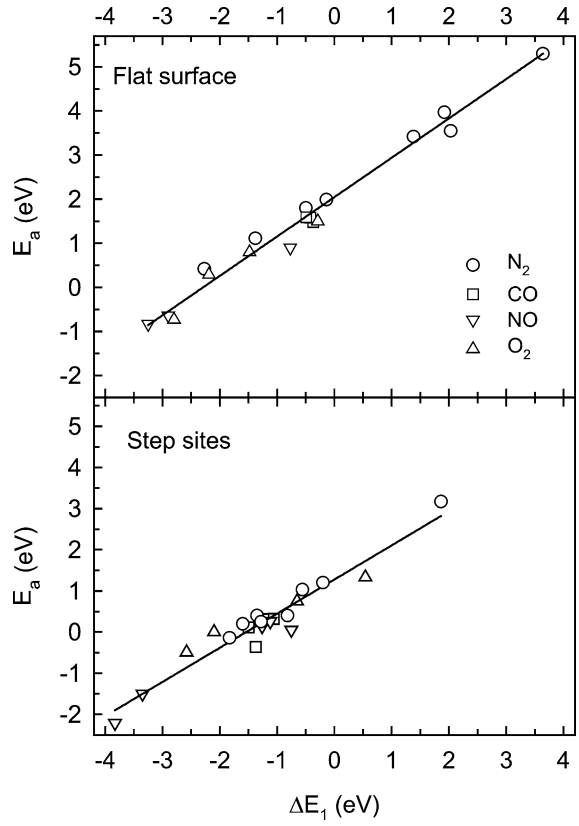

Fig. 1. Calculated transition state energies (E_a) and dissociative chemisorption energies (ΔE_1) for N_2, CO, NO, and O_2 on a number of transition metal surfaces. Results for close packed as well as stepped surfaces are shown. Adapted from Ref. [8].

density-functional theory (DFT) calculations that it has been possible to establish such relations firmly for a number of systems. An unexpected result from these calculations was the findings that not only do many surface reactions follow BEP relationships, there are classes of similar reactions which follow the same "universal" relationship [8]. This is illustrated for N_2, CO, NO, and O_2 dissociation in Fig. 1. Subsequent calculations have confirmed these results and have shown similar universal BEP relations to hold also for other surface reactions [12].

In the following it is shown that the linear BEP relationship in a number of cases leads directly to volcano curves where the fundamental parameter is the dissociative chemisorption energy of the key[2] reactant. We analyze several simple kinetic models to understand how the volcano curve depends on the mechanism and on the number of possible rate-determining steps. An important outcome of this analysis is that for a class of reactions involving key reactants that follows the same BEP relation, the maximum in the volcano curve is found generally to be in the same range of reaction energies, independent of the reaction, and that variations in the position of the maximum with reaction conditions can be understood in some detail.

The concepts developed here are tested by showing excellent agreement with experimental results for hydrogenation of CO to hydrocarbons, i.e., methanation and Fischer–Tropsch synthesis. We have synthesized a series of supported catalysts and determined their activity toward CO methanation. It is found that the measured activity plotted against the calculated dissociative CO chemisorption energy results in a very nice volcano curve with a maximum in the "universal range" [8] proposed by our analysis.

The main conclusion of this work is that the dissociative chemisorption energy is a good descriptor of the catalytic activity for a series of simple catalytic reactions. As an aid to understanding trends in catalytic activities for other reactions, we present systematic DFT calculations of reaction energies for molecular and dissociative chemisorption for a large number of molecules on stepped surfaces of the 13 transition metals most commonly used in heterogeneous catalysis.

2. Evaluation of four simple kinetic models

In the following the simplest possible surface-catalyzed reactions are considered. The aim here is not to describe any particular reaction in detail, but to bring out the basic parameters determining the reactivity. Later we will show that the general principles work well for real catalytic processes.

We will consider reactions, which can be viewed as activation (dissociation) of a key reactant followed by removal of the dissociation products by further reaction with a secondary reactant. Ammonia synthesis can, for instance, be viewed as activation of N_2 followed by removal of adsorbed N by hydrogen, Fischer–Tropsch synthesis is activation of CO, NO reduction is activation of NO, and oxidation reactions can be viewed as activation of O_2 followed by removal of oxygen from the surface by the reductant.

2.1. Case 1: Dissociative adsorption as rate-determining step

1. $A_2 + 2^* \leftrightarrows 2A^*$
2. $A^* + B \leftrightarrows AB + ^*$

It is assumed that A_2 binds weakly (or not at all) to the surface; hence the coverage of A_2 is negligible. We write reaction (2) as if the gas-phase molecule B reacts directly with an adsorbed atom A, but this reaction may involve several elementary steps, including adsorption of B. Then, the only approximation is that the coverage of B is negligible. This case is for instance analogous to ammonia synthesis under industrially relevant conditions (with A = N and B = $\frac{3}{2}H_2$). Let us assume in analogy with the ammonia synthesis reaction that the first step is rate determining. Then the rate of

[2] On the most active metals dissociation of the key reactant is rate determining.

the total reaction can be written

$$r(T, P_x) = 2k_1 P_{A_2} \theta_*^2 \left(1 - \frac{P_{AB}^2}{K_{eq} P_{A_2} P_B^2}\right) = 2k_1 P_{A_2} \theta_*^2 (1-\gamma). \quad (1)$$

Here

$$k_1 = \nu_1 e^{-E_a/k_B T} \quad (2)$$

is the rate constant for reaction (1) in the forward direction (note that the value of ν_1 is not important when discussing trends as long as it does not vary from one catalyst to the next [13]), $\gamma = P_{AB}^2/(K_{eq} P_{A_2} P_B^2)$ is the approach to equilibrium for the overall gas-phase reaction $A_2 + 2B \leftrightarrows 2AB$, and K_{eq} is the corresponding equilibrium constant.

Since reaction (2) is in equilibrium, the coverage of free sites is given by

$$\theta_* = \frac{1}{1+\frac{\theta_A}{\theta_*}} = \frac{1}{1+\frac{P_{AB}}{K_2 P_B}} = \frac{1}{1+\sqrt{K_1 P_{A_2} \gamma}}, \quad (3)$$

where

$$K_i = e^{\Delta S_i/k_B} e^{-\Delta E_i/k_B T} \quad (4)$$

is the equilibrium constant for reaction i, with corresponding reaction entropy, ΔS_i, and energy, ΔE_i.[3] In Eq. (3) we express the blocking of sites by adsorption of A atoms in terms of ΔE_1 instead of ΔE_2 by introducing the approach to equilibrium γ. This has the useful effect that all the variations from one catalyst to the next are described by E_a and ΔE_1 [see Eq. (1)].

The basic premises throughout the present work is that E_a and ΔE_1 are linearly related (Fig. 1),

$$E_a = \alpha_1 \Delta E_1 + \beta_1, \quad (5)$$

and we shall use the values $\alpha_1 = 0.87$ and $\beta_1 = 1.34$ eV as determined in Ref. [8] but the precise values of these constants are not important in the context presented here. The linear relationship means that the catalyst can be described by a single parameter, ΔE_1, while the most important effects having to do with the overall reaction and the reaction conditions are described by γ. Combining Eqs. (1), (2), (4), and (5) shows that *for Case* 1 *all reactions have the same kinetics as a function of* ΔE_1 *for a given approach to equilibrium.*

Since different reactions may be run with quite different approaches to equilibrium, we study the effect of varying γ. The result is shown in Fig. 2. There is a noticeable shift in the maximum to stronger bonding (more negative ΔE_1) when the approach to equilibrium becomes smaller. This means that for a given reaction, the choice of best catalyst depends on the approach to equilibrium as discussed in Ref. [14]. When comparing different reactions, it is worth noting that the more exothermic the gas-phase reaction, the larger K_{eq}, and the smaller the approach to equilibrium for a given conversion (given by $P_{AB}^2/(P_{A_2} P_B^2)$). This means that very exothermic reactions will have a maximum for metals with stronger binding energies (further to the left in the Periodic Table, see Table 1).

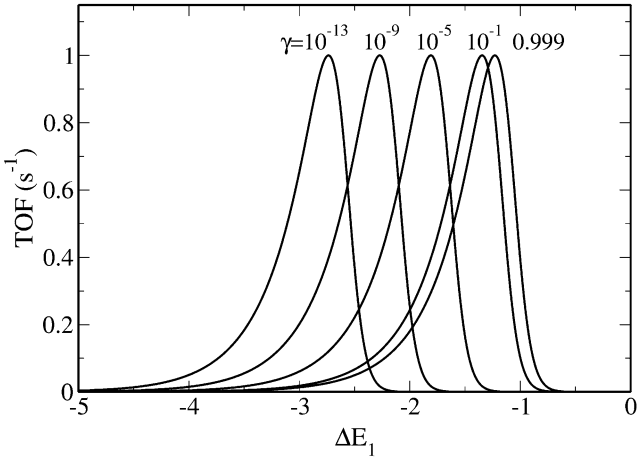

Fig. 2. Volcano plots (normalized turnover frequencies vs ΔE_1) for Case 1, values of $\gamma = 0.999$, 10^{-1}, 10^{-5}, 10^{-9}, and 10^{-13}. The parameters used are typical of a catalytic reaction: $T = 600$ K, $\Delta S_1 = 200$ J/(K mol), $P_{A_2} = 25$ bar. For equilibrium-limited reactions, such as ammonia synthesis, the approach to equilibrium will vary from 0 at the inlet of the reactor bed to ideally 1 at the outlet. The optimal catalyst thus depends on the position in the reactor bed (see Ref. [14]).

The results in Fig. 2 are for a typical set of parameters, $T = 600$ K, $\Delta S_1 = 200$ J/(K mol), $P_{A_2} = 25$ bar. The entropy loss due to adsorption, ΔS_1, is typical for molecular adsorption—since most degrees of freedom are frozen out at the surface, it is roughly given by the gas-phase entropy of the molecule, which is essentially independent of the molecule in question for simple gas-phase molecules [15].

To ensure that the results are not depending strongly on the other parameters we show in Fig. 3 how the position of the volcano depends on reaction conditions. The dependence is modest, but quite interesting. A low temperature process clearly needs a more noble catalyst (noble being short for a catalyst with a less negative value of ΔE_1) than a high-temperature process, the decisive factor being the availability of free sites on the surface rather than the activation of the reactant molecules. It should be noted, however, that for the type of active sites (a given BEP line) considered here it is difficult to exploit a low-temperature process even if a very noble (high ΔE_1) catalyst is used. This is because at the values of ΔE_1 where there are free sites on the surface, the activation of the reactants is so slow that the absolute values of the turnover rates are extremely low. Completely new active sites are needed for such processes, as, for instance, illustrated recently by the very small gold particles, which can be active even at room temperature [16–18].

[3] In the context of the trends discussed in this paper the difference between enthalpy and energy is insignificant and we will use energy everywhere.

Table 1
Calculated dissociative chemisorption energies for various molecules on a number of transition metal surfaces with respect to molecules in vacuum

	H_2	OH	N_2	CO	NO	O_2	H_20	$H_2O \rightarrow OH^* + 0.5H_2$	CO_2	NH_3	CH_4	$CH_4 \rightarrow C^* + 2H_2$
Fe	−1.15	−4.14	−1.27	−2.53	−4.66	−6.30	−1.98	−0.86	−2.51	−1.45	−1.07	1.24
Co	−0.78	−3.43	−0.38	−1.51	−3.63	−5.07	−0.99	−0.65	−0.83	−0.43	0.09	1.65
Ni	−0.82	−2.77	−0.10	−1.05	−2.87	−3.90	−0.45	−0.49	0.17	−0.37	−0.13	1.52
Cu	−0.29	−1.81	2.88	1.77	−0.68	−2.51	0.78	−0.07	3.69	1.92	3.06	3.64
Mo	−0.92	−4.61	−2.76	−3.61	−5.99	−7.48	−2.33	−1.20	−4.18	−1.84	−1.09	0.74
Ru	−1.09	−3.27	−0.84	−1.62	−3.60	−4.62	−1.08	−0.64	−0.77	−1.14	−0.88	1.30
Rh	−0.79	−2.82	−0.70	−1.12	−3.23	−4.03	−0.48	−0.27	0.03	−0.61	−0.06	1.51
Pd	−0.78	−1.40	1.78	0.38	−0.58	−1.20	0.95	0.36	2.96	0.64	0.04	1.60
Ag	0.53	−0.48	5.86	4.32	1.73	−0.65	2.52	0.52	7.16	4.63	6.31	5.26
W	−1.29	−5.37	−4.33	−4.73	−7.34	−8.62	−3.27	−1.45	−5.87	−3.18	−2.37	0.20
Ir	−1.26	−3.37	−0.59	−1.07	−3.49	−4.65	−1.26	−0.35	−0.23	−1.27	−0.65	1.87
Pt	−1.12	−2.06	1.37	0.37	−1.27	−2.17	0.12	0.25	2.45	−0.08	−0.18	2.07
Au	0.18	−0.05	5.89	4.58	2.34	0.54	2.77	0.92	8.02	4.12	5.28	4.92

The adsorption has been calculated on the fcc (211) surface in all cases except for Fe, Mo, and W, for which the calculations were done on bcc (210) surfaces. Zero point vibrational energies are not included. All energies are given in eV.

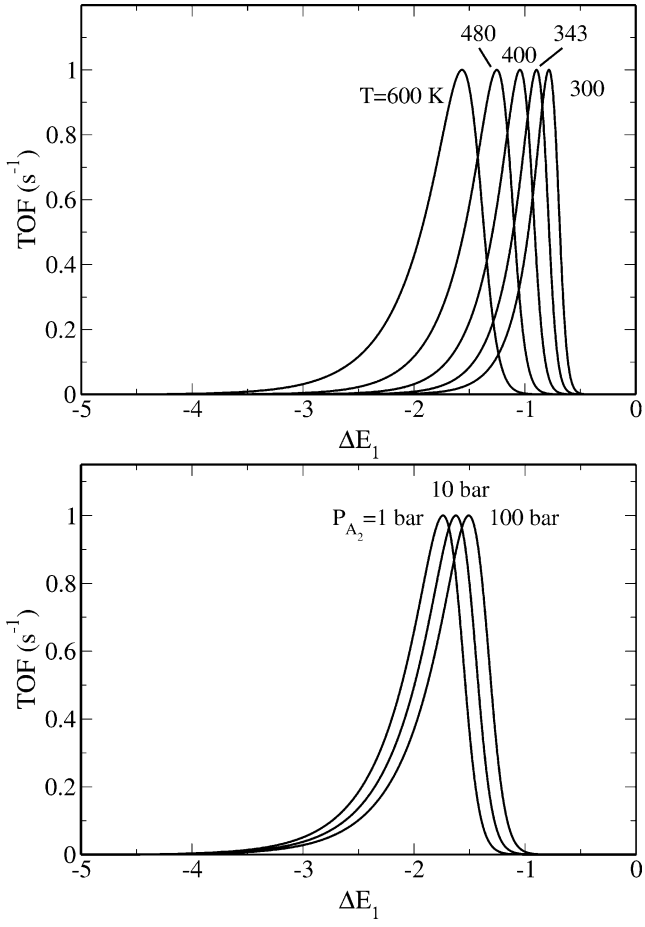

Fig. 3. Volcano plots (normalized turnover frequencies vs ΔE_1) for Case 1, when T and P_{A_2} are varied.

2.2. Case 2: Dissociative adsorption as rate-determining step with a strongly adsorbed molecular precursor

We now include the possibility of a strongly adsorbed molecular precursor.

1a. $A_2 + * \leftrightarrows A_2*$
1b. $A_2* + * \leftrightarrows 2A*$
2. $A* + B \leftrightarrows AB + *$

We still assume A_2 dissociation to be rate determining, but now the rate-determining step is a surface reaction, not the adsorption process. The rate is

$$r(T, P_x) = 2k_{1b}\theta_{A_2}\theta_*(1-\gamma). \tag{6}$$

The coverage of the molecularly adsorbed state is

$$\theta_{A_2} = \frac{K_{1a}P_{A_2}}{1 + \frac{P_{AB}}{K_2 P_B} + K_{1a}P_{A_2}} \tag{7}$$

and the coverage of free sites is

$$\theta_* = \frac{1}{1 + \frac{P_{AB}}{K_2 P_B} + K_{1a}P_{A_2}} = \frac{1}{1 + \sqrt{K_1 K_{1a} P_{A_2}\gamma} + K_{1a}P_{A_2}} \tag{8}$$

and

$$k_{1b} = \nu_{1b} e^{-(E_a - \Delta E_{1a})/k_B T}, \tag{9}$$

where now the activation energy of the dissociation is given by the transition state energy E_a and the molecular adsorption energy ΔE_{1a}.

Fig. 4. shows the calculated rate as a function of ΔE_1 for values of ΔE_{1a} between −0.75 and −2 eV. For values of ΔE_{1a} larger than −1 eV there is essentially no effect, but for stronger precursor bonding energies there is a considerable shift in the position of the maximum toward more reactive catalysts (more negative ΔE_1).

2.3. Case 3: Dissociative adsorption as rate-determining step followed by reaction with a strongly adsorbed species

In the cases considered until now, the coverage of B on the surface has been assumed to be unimportant. We now include the possibility that B is strongly adsorbed onto the surface.

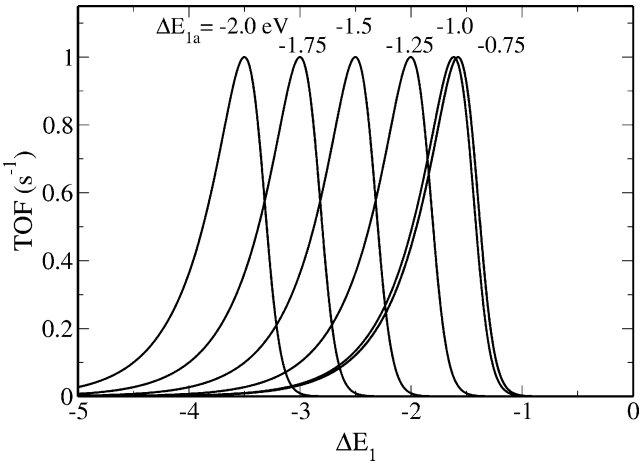

Fig. 4. Volcano plot (normalized turnover frequencies vs ΔE_1) for Case 2, $\Delta E_{1a} = -0.75$, -1.00, -1.25, -1.50, -1.75, and -2.0 eV.

1. $A_2 + {}^* \leftrightarrows 2A^*$
2a. $B + {}^* \leftrightarrows B^*$
2b. $A^* + B^* \leftrightarrows AB + {}^*$

We still assume A_2 dissociation to be rate determining:

$$r(T, P_x) = 2k_1 P_{A_2} \theta_*^2 (1 - \gamma). \tag{10}$$

The coverage of free sites is now given by

$$\theta_* = \frac{1}{1 + \sqrt{K_1 P_{A_2} \gamma} + K_{2a} P_B}. \tag{11}$$

In this case a shift in the volcano maximum toward more negative values of ΔE_1 (stronger bonding of A to the surface) appears when B binds stronger to the surface. The shift simply results from the competition of A and B adsorbates for sites on the surface, and it turns out that the kinetics behaves exactly as if B were a molecular precursor. The same will be true of any other adsorbate state competing for sites on the surface.

2.4. Case 4: Dissociative adsorption as rate-determining step followed by a reaction with two product-channels

We now examine the case of a hetero-nuclear reactant.

1. $AC + 2^* \leftrightarrows A^* + C^*$
2a. $A^* + B \leftrightarrows AB + {}^*$
2b. $C^* + B \leftrightarrows CB + {}^*$

This gives

$$\theta_* = \frac{1}{1 + \frac{P_{AB}}{K_{2a} P_B} + \frac{P_{CB}}{K_{2b} P_B}}. \tag{12}$$

Since the pressures of the two products must be the same, $P_{AB} = P_{CB} = P_{XB}$, the important part of the denominator can be written as

$$\frac{P_{AB}}{K_{2a} P_B} + \frac{P_{CB}}{K_{2b} P_B}$$

$$= \sqrt{K_1 P_{AC}} \sqrt{\frac{P_{AC}^2}{K_1 K_{2a} K_{2b} P_{AC} P_B^2}} \left(\sqrt{\frac{K_{2a}}{K_{2b}}} + \sqrt{\frac{K_{2b}}{K_{2a}}} \right)$$

$$= \sqrt{K_1 P_{AC} \gamma} \left(\sqrt{\frac{K_{2a}}{K_{2b}}} + \sqrt{\frac{K_{2b}}{K_{2a}}} \right). \tag{13}$$

Thus,

$$\left(\sqrt{\frac{K_{2a}}{K_{2b}}} + \sqrt{\frac{K_{2b}}{K_{2a}}} \right) = \sqrt{\xi} = 2 \cosh \left(\frac{\Delta E_{2a} - \Delta E_{2b}}{2kT} \right) \tag{14}$$

and when $|\Delta E_{2a} - \Delta E_{2b}| \gg 2kT$, we find that

$$\sqrt{\xi} \approx e^{|\Delta E_{2a} - \Delta E_{2b}|/2kT}. \tag{15}$$

For the coverage of free sites we have

$$\theta_* = \frac{1}{1 + \sqrt{K_1 P_{AC} \gamma \xi}}, \tag{16}$$

meaning that we have now separated the coverage term into a term describing the properties of the reactant (K_1 or, equivalently, ΔE_1), one describing the overall gas-phase reaction (γ), and one describing the heterogeneity of the products (ξ). In most cases ΔE_1 will capture the main trends from one catalyst to the next, see Fig. 2. Since in most cases (CO or NO hydrogenation, for instance) $\xi \gg 1$, this factor will tend to compensate γ.

We conclude that the simplest possible kinetic models of a surface-catalyzed reaction with a single rate-determining step directly lead to the dissociative chemisorption energy as the natural measure of the reactivity. The reason is the obvious one, that the two parameters characterizing the kinetics, the activation energy E_a of the rate-determining step and the dissociative chemisorption energy, ΔE_1, are linearly related.

The assumption of a single rate-determining step, may, however be too restrictive as discussed for instance by Campbell [19] and Dumesic [20,21]. We will therefore in the following discuss how much this picture changes if we relax the assumption that there is only a single rate-determining step.

3. Reactions with competing rate-determining steps

We now return to Case 1, but make no assumption about the relative approaches to equilibrium of steps (1) and (2). A schematic illustration of the reaction potential energy diagram is shown in Fig. 5. In Case 1 there are only two steps, but the analysis below will also describe reactions where there are several steps and two of them, adsorption and some other surface reaction step following that, can simultaneously be rate determining. For the case of CO hydrogenation, for instance, we could be looking at CO dissociation and another step, such as adsorbed C reacting with hydrogen, see Fig. 6.

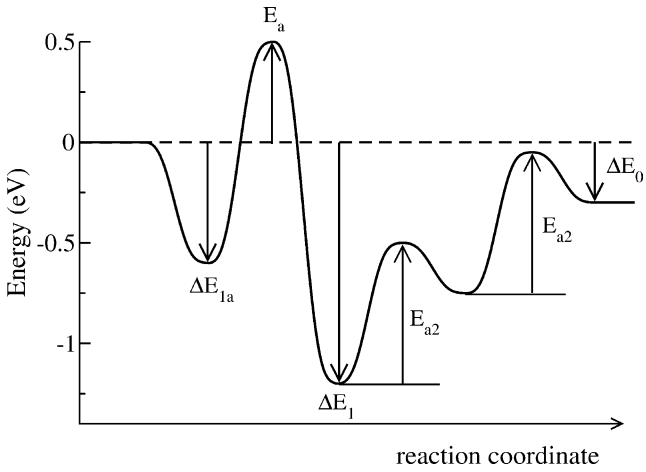

Fig. 5. Schematic potential energy diagram for a surface reaction involving adsorption of A_2, dissociation of A_2, and two times reaction with B to form two AB molecules from A_2 and 2B.

We write the net rates of the two reaction steps as we assume that the coverage of A_2 is negligible:

$$r_1 = 2k_1 P_{A_2}\theta_*^2 - 2k_{-1}\theta_A^2 = 2k_1 P_{A_2}\theta_*^2\left(1 - \frac{k_{-1}\theta_A^2}{k_1 P_{A_2}\theta_*^2}\right) = 2k_1 P_{A_2}\theta_*^2(1-\gamma_1), \quad (17)$$

$$r_2 = k_2 P_B\theta_A - k_{-2}P_{AB}\theta_* = k_2 P_B\theta_A\left(1 - \frac{k_{-2}P_{AB}\theta_*}{k_2 P_B\theta_A}\right) = k_2 P_B\theta_A(1-\gamma_2), \quad (18)$$

where we have introduced the "approaches to equilibrium" for each step, γ_1 and γ_2. These variables, which are also frequently called the "reversibilities" [20], describe how close each reaction step is to equilibrium in the "de Donder" sense [22]. In the stationary coverage situation, which we shall assume throughout, it is evident that the net rate of reaction (2) is the same as that of reaction (1), as reaction (1) describes the net production of sites covered with atom A due to dissociative adsorption, and reaction (2) describes the net removal of A atoms from the surface due to desorption. The rates r_1 and r_2 are thus equivalent descriptions of the total rate of the catalytic process. The exact solution of the microkinetic model is obtained by numerically solving the Eqs. (17), (18) under the constraint of site conservation.

The rate constants, $k_1 = \nu_1 e^{-E_a/k_B T}$, $k_{-1} = \nu_{-1} \times e^{-E_{a-}/k_B T}$, $k_2 = \nu_2 e^{-E_{a2}/k_B T}$, and $k_{-2} = \nu_{-2} e^{-E_{a2-}/k_B T}$ are given by the activation energies, as indicated in Fig. 5, and from some simple assumptions about the reaction entropies which are discussed below. The activation energy for adsorption is discussed above. In the present case we also need those for the forward and backward surface reaction, E_{a2} and E_{a2-}. For the forward rate we assume in analogy with Eq. (5) that there is a BEP relation,

$$E_{a2} = \alpha_2 \Delta E_1 + \beta_2, \quad (19)$$

where now α_2 is negative, such that the stronger A bonds to the surface, the higher the activation energy. If step (2) is desorption of a simple molecule then the expression for E_{a2} above describes exactly the inverse of Eq. (5), and we must have $\alpha_2 = \alpha_1 - 1$, where α_1 is the coefficient in the

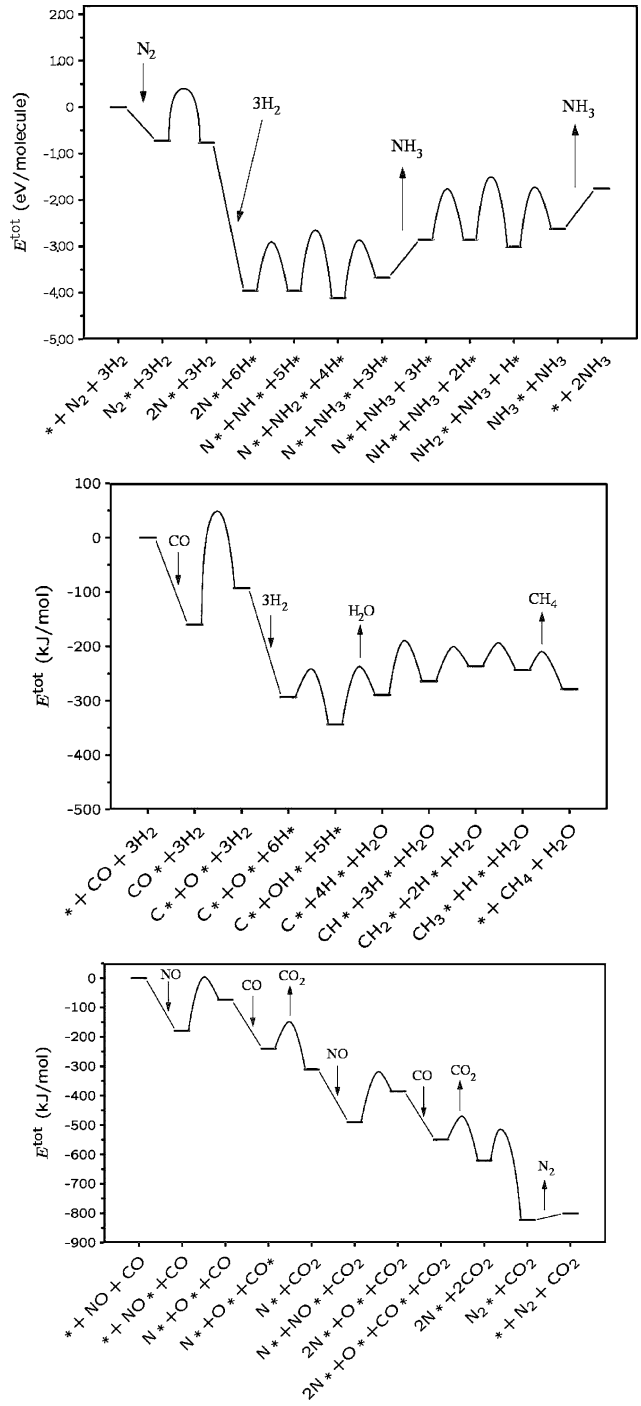

Fig. 6. Comparison of calculated potential energy diagrams for ammonia synthesis over stepped Ru (top), from Logadottir and Nørskov [24]; CO hydrogenation over stepped Ni (middle), adapted from Bengaard et al. [25]; NO reduction by CO over stepped Pd (bottom), adapted from Hammer [26]. Note, that in all cases dissociation of the main reactant is followed by unactivated adsorption of the other reactant and removal of the product. The latter process is associated with reaction barriers on the order of 1 eV in all cases.

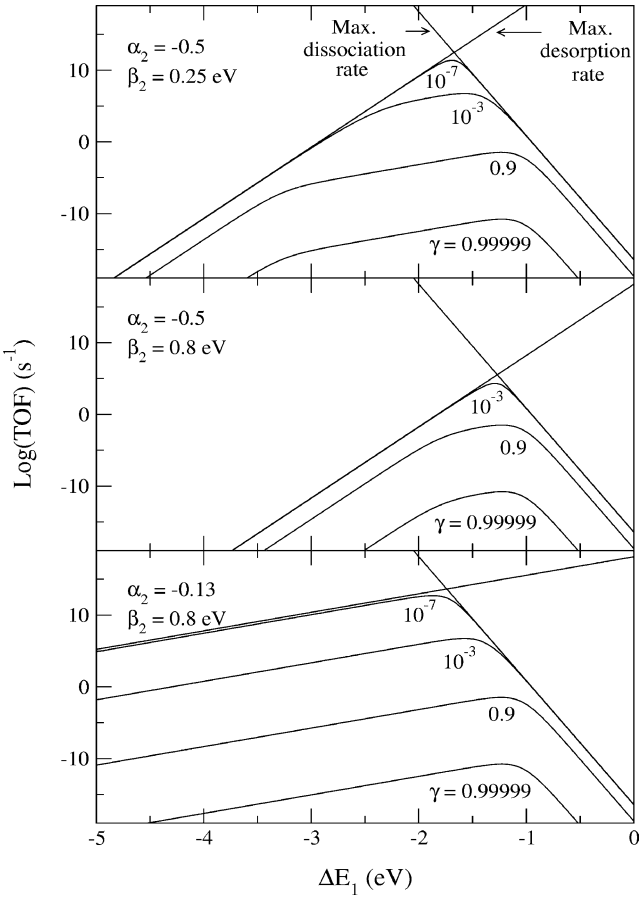

Fig. 7. The Sabatier volcano curve for $\gamma = 0$ and the real volcano curves for various values of γ. The parameters for α_2 and β_2 are shown. One of the values chosen is $\alpha_2 = \alpha_1 - 1 = -0.13$ using the value of α_1 from Fig. 1. We have assumed that the reaction enthalpy of the total gas-phase reaction is $\Delta E_0 = -1$ eV, but that does not affect the Sabatier curves, only the approaches to equilibrium.

BEP relation for the dissociative adsorption of molecule AB. E_{a-} is given from ΔE_1 and E_a and similarly E_{a2-} is given from E_{a2}, ΔE_1, and the reaction enthalpy of the gas phase reaction, ΔE_0; see Fig. 5.

The surface reaction prefactors ν_{-1} and ν_2, for redesorption of A_2 and forward reaction of AB, respectively, have both been set to $(k_B T)/h$, which results from assuming negligible entropy of the adsorped species and a strongly constrained transition state with a partition function of unity [23]. The gas reaction prefactors ν_1 and ν_{-2} are then determined under the assumption of zero reaction entropy of step (2) and by assuming a gas-phase entropy of diatomic molecules of 200 J/(K mol). The former assumption turns out to only have a very limited effect on the position of the maximum of the volcano curve, while the latter assumption is approximately valid for all of the relevant diatomic molecules [15].

In Fig. 7 the solutions of the microkinetic model for three different sets of parameters are shown. The calculated potential energy surfaces in Fig. 6 [24–26] show an activation barrier for further surface reaction, E_{a2}, of the order 1.0 to 1.5 eV. All the cases included in Fig. 6 are for catalyst surfaces close to the optimum, with values of ΔE_1 in the range from -1.0 to -1.5 eV. This limits the variation of α_2 and β_2, and the cases included in Fig. 7 all give activation barriers in the range dictated by the three reactions in Fig. 6.

Comparing the volcano curves of Fig. 7 to those of Fig. 2, the main difference is that at adequately negative values of ΔE_1 there is a break in the volcano curves because the surface reaction ($A + B \rightarrow AB$) becomes rate determining. The more activated the second reaction, the further the maximum moves to the right. This means that the inclusion of the possibility of a second rate-limiting step removes a large part of the shift in the maximum of the volcano curves for reactions very far from equilibrium and for reactions with strongly bound molecular precursors. This means that the largest shift in the maximum of the volcano to negative values of ΔE_1 for reactions very far from equilibrium is eliminated.

We note that independent of the exact value of the parameters α_2 and β_2, the maximum in rate is observed to be catalysts that provides dissociative chemisorption energies in the range $\Delta E_1 = -1.0 - -2.0$ eV. While this might appear as a broad range, it typically spans only two neighbors in the Periodic Table, cf. Table 1. The differences in ΔE_1 for CO or N_2 from one surface to the next surface to the right or left in the Periodic Table is 0.5–1.0 eV. This range therefore defines the best catalysts quite well.

In order to understand the results in Fig. 7 and in order to be able to treat the general case with more than two possible rate-determining steps, we consider a limiting behavior closely related to the Sabatier principle [27]. The Sabatier principle states that the catalytic activity for a given reaction follows a volcano curve through the Periodic Table, because an intermediate binding of reaction intermediates to the surface will give an optimal catalyst. The usual interpretation is that for very reactive surfaces, the rate-determining step will be desorption of product molecules from the surface, while the rate-determining step for more noble surfaces will be the dissociative chemisorption of reactants [27]. This suggests that the optimal catalytic surface is a surface where there is competition between dissociation and desorption, with a maximum turnover frequency at the point of switching between free and occupied sites.

Inspecting Case 1 again, a simplified solution, which we shall denote the Sabatier analysis, is obtained as follows. We define the approach to equilibrium for the combined reaction,

$$\gamma = \frac{P_{AB}^2}{K_{eq} P_{A_2} P_B^2}, \tag{20}$$

and use that

$$K_{eq} = K_1 K_2^2 \tag{21}$$

or

$$\gamma = \gamma_1 \gamma_2^2. \tag{22}$$

If we limit our interest to net reactions proceeding in the forward direction, we have

$$0 \leqslant \gamma \leqslant 1, \quad 0 \leqslant \gamma_1 \leqslant 1, \quad 0 \leqslant \gamma_2 \leqslant 1. \tag{23}$$

Together with the Eq. (22) above, this implies

$$0 \leqslant \gamma \leqslant \gamma_1 \leqslant 1 \quad \text{and} \quad 0 \leqslant \gamma \leqslant \gamma_2^2 \leqslant 1. \tag{24}$$

Now the Sabatier principle can be stated in mathematical terms for Case 1. When a reactive surface is used as the catalyst, the surface coverage will be high ($\theta_A \approx 1$) and the desorption reaction will be the rate-determining step ($\gamma_1 \approx 1$ and $\gamma_2 \approx \sqrt{\gamma}$). The net turnover frequency of the reaction should be well approximated by

$$r = k_2 P_B\big(1 - \sqrt{\gamma}\big). \tag{25}$$

On the other side of the peak of the volcano, dissociative chemisorption is rate determining ($\gamma_1 \approx \gamma$ and $\gamma_2 \approx 1$) and the coverage of free sites dominates ($\theta_* \approx 1$). The turnover frequency should here be well described by

$$r = 2k_1 P_{A_2}(1 - \gamma). \tag{26}$$

Because each coverage has an upper bound of 1, the total rate must be bounded by both (25) and (26). This gives a volcano

$$r = \min\big(2k_1 P_{A_2}(1 - \gamma), k_2 P_B\big(1 - \sqrt{\gamma}\big)\big), \tag{27}$$

which we shall refer to as the Sabatier volcano curve.

In Fig. 7, it can be seen that the Sabatier volcano gives an excellent description of the corresponding microkinetic model in the case where $\gamma \to 0$. The only discrepancy occurs near the top of the volcano, where the Sabatier analysis, as we have constructed it here, fails to describe the switching of coverage. In general the Sabatier principle holds very well for the simple kinetic model as long as the approach to equilibrium is small. It is also seen in Fig. 7 that close to equilibrium, $\gamma \to 1$, the optimal catalyst is not defined by the position of the maximum of the Sabatier volcano. In this case the optimum moves toward more noble surfaces, and the optimum is here well determined by a microkinetic model that assumes dissociation is the rate-determining step.

For a microkinetic model with more than just two reaction steps, a Sabatier analysis could be constructed in analogy with the one presented here:

- Assume optimal coverages of all intermediates going into the forward rates.
- Calculate the approach to equilibrium for each forward rate from the given approach to equilibrium for the overall reaction, while assuming that all other partial reactions are in equilibrium.
- Calculate the rate-constants going into each forward rate, from the known BEP relationships for the given intermediates.

This gives a first approximation to each forward rate, and the "Sabatier volcano" is constructed by setting the total rate equal to the minimum of all forward rates at each value of the parameter describing the surface reactivity, which in our case is the dissociative chemisorption energy of the reactant. In general, such a Sabatier volcano would then be convex and could have more than just the two usual sides corresponding to desorption and dissociation limitation. If more than one independent parameter is needed to describe the model, the volcano will in general become a prism.

We conclude that the inclusion of more than one rate determining step does not change the general conclusion that ΔE_1 is a good parameter for characterizing the catalytic activity of a metal catalyst, given that the reaction follows a BEP relation as in Eq. (19). With the values chosen here, corresponding to the universal BEP for the strongly bound diatomic molecules (that includes N_2, CO, O_2, and NO), the optimal catalysts have values of ΔE_1 in the range from -1 to -2 eV.

From this analysis it is clearly important to have access to systematic databases of dissociative chemisorption energies. In the following we present such a database calculated using DFT. Even if the absolute accuracy of such calculations is limited to about 0.2–0.3 eV [28] trends are generally well described [11], and that is the most important in the present context.

4. The surface thermo-chemistry database

The DFT calculations were performed within a plane-wave pseudopotential implementation [29,30]. We used the ultrasoft pseudopotentials of Vanderbilt [31] to represent the ionic cores, allowing for a good treatment of first-row atoms and transition metals with a relatively limited plane-wave basis. The plane-wave cutoff in the calculations was 25 Ry in all cases, except for the cobalt surface, in which case a cutoff of 35 Ry was chosen, due to the hardness of the corresponding pseudopotential. All calculations were performed with the RPBE exchange-correlation functional [28] on periodically repeated stepped metal slabs. The surface coverage of the adsorbates was 1/6 in all cases, and the slab thickness was 9 layers in the [211] direction for the fcc metals and 11 layers in the [210] direction for the bcc metals. In the case of the hcp metals (Ru and Co), the adsorption was modeled by using the same type of fcc (211) slabs as for the fcc metals. The fcc and the bcc surfaces exposed a terrace of close-packed atoms, the (111) and (110) layers respectively, and the uppermost close-packed layer, including the step atoms were in all cases fully relaxed together with the adsorbate atom/molecule. These stepped surfaces have been chosen for maximal computational ease. Other steps and crystal structures may lead to slightly different chemisorption properties. The choice of the bcc (210) surface is expected to lead to more stable chemisorption states than if a more close-packed surface was used. N_2 for example has a

Table 2
Calculated associative molecular chemisorption energies determined by DFT with respect to molecules in vacuum

	OH	N_2	CO	NO
Fe	−3.60	−0.35	−1.52	−2.34
Co	−3.48	−0.47	−1.50	−2.13
Ni	−3.23	−0.47	−1.66	−2.10
Cu	−2.81	0.07	−0.62	−0.71
Mo	−3.94	−0.24	−1.60	−2.59
Ru	−3.37	−0.61	−1.77	−2.35
Rh	−3.00	−0.56	−1.79	−2.16
Pd	−2.38	−0.25	−1.74	−1.79
Ag	−2.22	0.04	−0.06	−0.08
W	−4.19	−0.50	−2.02	−2.81
Ir	−3.08	−0.69	−1.96	−2.32
Pt	−2.49	−0.24	−1.89	−1.91
Au	−1.81	0.05	−0.35	−0.22

The adsorption has been calculated on the fcc (211) surface in all cases except for Fe, Mo, and W, for which the calculations were done on bcc (210) surfaces. Zero point vibrational energies are not included. All energies are given in eV.

dissociative chemisorption energy of −2.76 eV on the (210) Mo surface, whereas the corresponding energy on the (321) Mo surface is −1.86 eV. The lattice constants were chosen as the calculated bulk lattice constant for the respective metals in their ground state structure using the RPBE functional. This avoids reminiscent stress in the calculational setup. Between the metal slabs we introduced at least 8 Å of vacuum, and the interaction between the dipole moments of the periodically repeated slabs was decoupled, by the introduction of a dipole layer in the vacuum between the slabs [32]. We used a **k**-point sampling of $4 \times 4 \times 1$ Monkhorst–Pack special points [33] in the x, y, and z directions, respectively; the number of **k** points was reduced to 8 **k** points in the irreducible Brillouin zone by time–inversion symmetry.

In the present calculations we have focused on systematically using the same accuracy in the calculation in terms of number of layers, size of the unit cell, number of **k** points, etc. Some of the results may therefore differ slightly from earlier compilations of a number of different calculations [8] due to differences in the number of layers, in the amount of relaxation, and whether the self-consistent calculations are done using one exchange correlation functional or another.

The results for dissociative chemisorption energies for a number of transition metals are shown in Table 1. In Table 2, molecular adsorption energies are tabulated for comparison. A detailed comparison to available experimental values and a discussion of trends will be presented elsewhere (T. Bligaard, J.K. Nørskov, to be published).

The concepts developed here have already been tested extensively on ammonia synthesis [11,14]. In order to show that they are more generally useful, we test them here by considering another important reaction, the methane synthesis from hydrogen and carbon monoxide. We have made a systematic series of catalysts and measured their catalytic activity under comparable conditions and will show that if these new data are plotted against the calculated dissociative chemisorption energies for CO from Table 1, a very nice volcano results with a maximum around −1.4 eV in perfect agreement with the present analysis.

5. Application to methanation

Most of the catalysts considered here were made by impregnation of 2-mm tablets of an alumina-stabilized MgO support material (Mg:Al = 7:1) with a surface area of 35 m^2/g. Aqueous solutions of $Ni(NO_3)_2$, $Pd(NH_3)_4(HCO_3)_2$, $Pt(NH_3)_4(HCO_3)_2$, $Rh(NO_3)_3$, NH_4ReO_4, $IrCl_3$, $RuNO(NO_3)_3$, $Fe(NO_3)_3$, and $Co(NO_3)_2$ were used. The impregnated supports were all dried overnight at 80 °C, except for the Ni catalyst, which was heated to 450 °C for 1 h and the Ru catalyst, which was dried at room temperature to avoid the creation of RuO_4. The metal concentrations were analyzed and were between 1 and 2 wt% metal for all catalysts, except for the Ni catalyst where the concentration was just over 3 wt%. See Table 3 for exact metal loadings.

Two different experimental setups were used to determine the methanation activities of the catalysts**.** One test unit was a differential flow reactor system previously described in detail [34]. A U-tube glass-lined stainless-steel reactor (i.d. 4 mm) was loaded with 100–200 mg of the catalysts (particle size 300–600 μm), which were fixed between two quartz wool wads. The inlet gas consisted of 1% CO in hydrogen and the inlet flow was 100 cm^3/min (NTP). The low CO concentration was chosen in order to suppress formation of heavier hydrocarbons than methane [35]. A pump delivered a recirculation flow rate of about 6000 cm^3/min (NTP) ensuring well-mixed conditions. The total pressure in the reactor was set at 1.5 bars and the CO and CO_2 concentration in the reactor effluent was monitored with a calibrated BINOS infrared detector. A blank test at 500 °C showed that the reactor system itself had no significant CO hydrogenation activity. Before activity measurements, the catalysts were reduced in flowing hydrogen (50 ml/min NTP) at 500 °C for 10 h. Each run consisted of a series of measurements of the steady-state CO and CO_2 concentrations at different temperatures starting at 200 °C and stopping when the CO conversions were close to 100%.

The second test unit was an integral plug-flow reactor system. The reactor was a U-tube made of quartz. It was loaded with 100–200 mg of catalyst, 150–300 μm sieved fraction. Inlet flows were 60, 120, and 200 cm^3/min (NTP) and the feed gas was again 1% CO in hydrogen. Each run started with a reduction of the catalyst in hydrogen (100 ml/min NTP) at 500 °C for 2 h. Reducing the Fe catalyst at 500 °C for 30 h instead of 2 had no effect on the activity. The reactor pressure was about 1.0–1.2 bar and the reactor effluent compositions were determined with a calibrated mass spectrometer. The catalyst activities were measured at temperatures ranging from 200 to 550 °C.

Table 3
Metal contents in the different supported catalysts

Catalyst	Re	Fe	Co	Ru	Rh	Ni	Ir	Pd	Pt
Metal load (wt%)	1.64	0.64	2.12	1.87	1.71	3.47	1.51	1.34	1.14

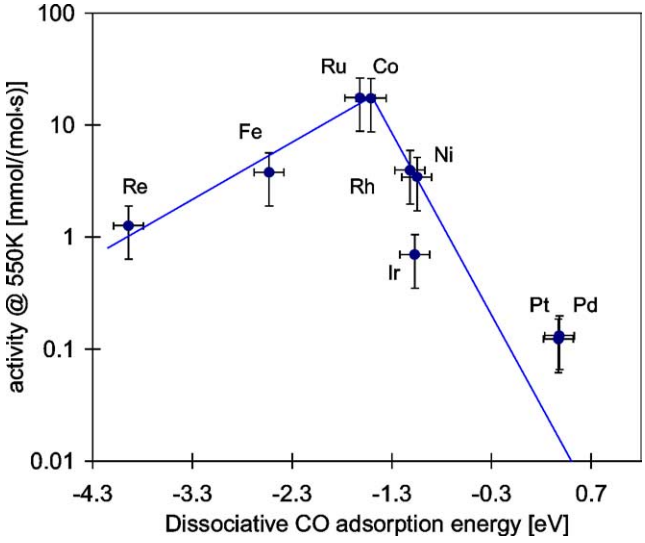

Fig. 8. Activities of different supported transition metals as a function of the reaction energy for dissociative CO chemisorption. See text for details. The uncertainty of the calculated adsorption energies is estimated from experience to be 0.15 eV, while the uncertainty of the activities is mostly related to not knowing the exact number of active step sites. The dissociative chemisorption energy for CO on Re, which is not included in the database, has been calculated to be −3.94 eV. The step on the Re surface was modeled by a fcc (211) slab.

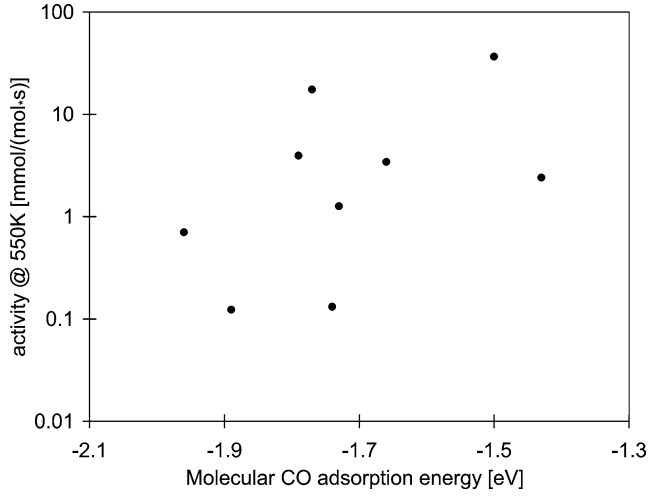

Fig. 9. Activities of different supported transition metals as a function of molecular CO chemisorption energies.

For the differential reactor system, activities were determined from inlet and effluent CO concentrations (conversion of CO to CO_2 was negligible in all experiments), while for the integral flow reactor system the activities were determined from the effluent CH_4 concentration. It was evident from the measurements that methane was the only hydrocarbon formed in significant amounts; i.e., the two ways of determining the activity give equal results. The data were analyzed assuming a reaction order in CO and CH_4 equal to zero for all metals and the reaction order in hydrogen is not important since the hydrogen pressure is practically constant during the experiments. These assumptions about the kinetics are supported by the observation that analyzing the data obtained at different inlet flows from the integral reactor gives rise to very similar results. To enable a comparison of the activities at the same temperature, activation energies were determined based on measurements where the CO conversion was below 80%. All activities were determined with respect to the quantity of metal contained in the catalyst.

The measured CO methanation activities as a function of the calculated values of ΔE_1 for dissociative CO adsorption at 550 K are shown in Fig. 8. There is a clear volcano relation. What is more, the maximum of the volcano is approximately at a dissociative adsorption energy of -1.4 eV, which is in very good agreement with the prediction above [8].

Although obtained for different catalysts (silica-supported transition metals) under different conditions ($CO:H_2 = 1:3$) the experimental CO hydrogenation data of Vannice [7] show the same trend in activity when plotted against the same reaction energy showing that the general concept is not dependent on the details of the catalyst preparation or the measurement of the catalytic activity. The absolute values of the activities are also similar indicating that the assumption of a reaction order in CO of zero is good. Since heavier hydrocarbons than methane were formed in the experiments of Vannice [7] it is evident that the volcano curve is also valid for Fischer–Tropsch synthesis.

Vannice [7] suggested correlating the catalytic activity to the molecular CO adsorption energy. When that is done using molecular adsorption energies from Table 2 there is no significant correlation; see Fig. 9. This is a clear indication that the dissociative adsorption energy is the important parameter in the problem—this is the energy, which is linearly correlated with the activation barrier for CO dissociation.

It would be more correct to plot the activity as turnover frequencies. However, this is difficult since the DFT calculations clearly show that it is only sites similar to the open sites found at the steps on the most close packed surfaces that are active for the CO dissociation reaction [8]. Molecular N_2 chemisorption at room temperature can be used to determine the density of such sites in the case of nickel-based catalysts, but there is no general method that can be used for all catalysts. Vannice [7] determined the total metal surface area using both molecular CO and dissociative H_2 chemisorption, which, for unknown reasons, for some of the metals resulted in quite different metal surface areas. How-

ever, plotting turnover frequencies based on these areas does not change the general shape of the volcano curve.

6. Concluding remarks

In the present paper we have investigated the kinetic consequences of the recent quantitative confirmation of the existence of Brønsted–Evans–Polanyi–type relations between the activation energy for dissociation and the dissociative chemisorption energy for a number of diatomic molecules. Using simple "generic" models of surface-catalyzed reactions we have shown that the dissociative chemisorption energy, which is the reaction energy of the rate-determining reaction, is usually a good descriptor of the catalytic activity of a given metal in the sense that if the activity is plotted as a function of this descriptor, a very reasonable volcano-curve results. There are, however, dependencies on temperature, pressure, and approach to equilibrium, and we have systematically investigated these.

We have also presented extensive databases of the adsorption energies, calculated using DFT.

It has been shown recently that a class of adsorption reactions follows the same "universal" Brønsted–Evans–Polanyi relation [8]. We have shown that if this relation is used in the kinetics, it turns out that in most cases the optimal adsorption energy (giving the largest catalytic activity) is in the range from -1 to -2 eV. As suggested in Ref. [8] this means that the universal Brønsted–Evans–Polanyi relation turns into a universal criterion for the optimal catalysts for all reactions belonging to the class.

The present analysis is simple and qualitative, but it explains reactivity trends for a number of reactions. We have shown how it can be used quantitatively to understand the volcano curve for the methanation reaction. All the best catalysts for CO hydrogenation have dissociative adsorption energies in the range from -1.0 to -1.6 eV. Similarly the best catalysts for N_2 hydrogenation (ammonia synthesis) have dissociative N_2 adsorption energies of -0.84 eV (Ru) and -1.27 eV (Fe) [36], the best catalyst for NO hydrogenation has a dissociative NO adsorption energy of -1.27 (Pt) [37], and the preferred catalyst for O_2 hydrogenation has a dissociative adsorption energy of -2.17 eV (Pt) [38] (there are no pure metals with an O_2 dissociative adsorption energy in the range from -1 to -2 eV).

The present analysis only deals with catalytic activity. For reactions where selectivity plays a role, the considerations above cannot be used. While Pt has the largest turnover for NO hydrogenation, Rh has a much larger selectivity for N_2 formation [37], which makes Rh a more interesting catalyst. Another factor that is not included here is the possibility that certain sites are poisoned during synthesis. Pt steps bind CO much stronger than the terraces, while this is less of a problem for Rh [39] and not a problem at all for Pd [24]. Such factors may, for instance, be important in making Pt less interesting than the two other metals as catalysts for the NO–CO reaction [40–42].

It is interesting to note that the volcano curves generated from the BEP relations are broad—a typical width is of the order 1 eV; see Fig. 7. Whereas the rates of the individual elementary steps vary on a thermal energy scale (an order of magnitude in rate corresponds roughly to an energy of $2k_BT$), the net rate varies much more slowly. This is a direct consequence of the fact that around the maximum in the volcano, the net rate is a competition between fast adsorption (being helped by stronger bonds to the surface) and fast surface reaction/desorption (being helped by weaker bonds to the surface). This weak dependence on the adsorption energy can be directly observed in the experimental data for CO hydrogenation in Fig. 8, and it is more generally observable in the fact that if a certain metal is a good catalyst for a reaction the neighbor in the periodic table is usually also reasonable. Since typical differences in adsorption energy between neighbors in the periodic table are also of the order 1 eV (see Table 1), this is the energy scale over which the net rate changes. This means that the accuracy we have in the DFT calculations is ample for obtaining reliable trends in reactivity.

It has been observed that the inclusion of adsorbate-adsorbate interactions at higher coverage may simply move the appropriate point along the BEP line [8,43]. The reason is that the transition state and the final state in dissociation are quite alike (this is the reason for the linear relation in the first place) [8], and the two states are therefore affected by high coverage in a similar manner. Weak adsorbate-adsorbate interactions following the BEP line with a strength considerably smaller than the width of the volcano (a few tenths of an eV or a few times 10 kJ/mol) will only have a weak effect on the results. If on the other hand the adsorbate–adsorbate interactions are larger than the width of the volcano, they may shift a metal in the interesting range of adsorption energies completely out of the interesting window of energies close to the maximum. This means that sites on the surface with high coverage are catalytically inactive and only sites with a low local coverage are active. This is implicitly what is treated in the simple mean field models treated above. Very reactive metals (far to the left of the maximum) may in a similar way be shifted into the interesting range by forming, e.g., oxides, nitrides, or carbides.

We also note that deviations from the linear BEP-relation would mean the breakdown of the compensation between faster adsorption and surface reactions, which gives rise to the smooth variation in the rate. There are deviations in the calculated values (see Fig. 1), but they are all small compared to the inherent accuracy of the calculations and we therefore cannot attach strong significance to them at the moment. The fact that many experiments show a smooth behavior of the reactivity across the periodic table is further testament to the notion that the linear BEP relationship is a very good starting point for understanding trends. It is, however, extremely important and interesting to look for devi-

ations from the linear relationships. One way to outperform the BEP curve reactions is to find new surface structures with different BEP lines. Another way is to include promoters. Adsorbed alkalis thus affect the barrier for N_2 dissociation more than the stability of the dissociation products (because the former has a larger dipole moment) leading to new active sites [44].

Finally, we have shown that reactions close to equilibrium tend to be dominated by a single rate-determining step and this determines the volcano curve. Far from equilibrium, on the other hand, we have introduced the Sabatier analysis, where the optimum is determined by the competition between fast adsorption and fast further reaction of the dissociation products.

Acknowledgments

We thank Galen B. Fisher for an enlightening discussion on NO decomposition. The Center for Atomic-Scale Materials Physics is sponsored by the Danish National Research Foundation, and the DFT calculations have been performed with support from the Danish Center for Scientific Computing through Grant HDW-1101-05.

References

[1] M. Boudart, in: G. Ertl, H. Knözinger, J. Weitkamp (Eds.), Handbook of Heterogeneous Catalysis, Wiley–VCH, Weinheim, 1997.
[2] J.A. Dumesic, D.F. Rudd, L.M. Aparicio, J.E. Rekoske, A.A. Treviño, The Microkinetics of Heterogeneous Catalysis, Am. Chem. Soc., Washington, DC, 1993, and references therein.
[3] M. Boudart, G. Djéga-Mariadassou, Kinetics of Heterogeneous Catalytic Reactions, Princeton Univ. Press, Princeton, NJ, 1984.
[4] C.J.H. Jacobsen, S. Dahl, B.S. Clausen, S. Bahn, A. Logadottir, J.K. Nørskov, J. Am. Chem. Soc. 123 (2001) 8404.
[5] H. Toulhoat, P. Raybaud, J. Catal. 216 (2003) 63.
[6] M.A. Barteau, Catal. Lett. 8 (1991) 175.
[7] M.A. Vannice, J. Catal. 50 (1977) 228.
[8] J.K. Nørskov, T. Bligaard, A. Logadottir, S. Bahn, M. Bollinger, L.B. Hansen, H. Bengaard, B. Hammer, Z. Sljivancanin, M. Mavrikakis, Y. Xu, S. Dahl, C.J.H. Jacobsen, J. Catal. 209 (2002) 275.
[9] V. Pallasana, M. Neurock, J. Catal. 191 (2000) 301.
[10] Z.-P. Liu, P. Hu, J. Chem. Phys. 114 (2001) 8244.
[11] A. Logadottir, T.H. Rod, J.K. Nørskov, B. Hammer, S. Dahl, C.J.H. Jacobsen, J. Catal. 197 (2001) 229.
[12] A. Michaelides, Z.-P. Liu, C.J. Zhang, A. Alavi, D.A. King, P. Hu, J. Am. Chem. Soc. 125 (2003) 3704.
[13] T. Bligaard, K. Honkala, A. Logadottir, J.K. Nørskov, S. Dahl, C.J.H. Jacobsen, J. Phys. Chem. B 107 (2003) 9325.
[14] C.J.H. Jacobsen, S. Dahl, A. Boisen, B.S. Clausen, H. Topsøe, A. Logadottir, J.K. Nørskov, J. Catal. 205 (2002) 382.
[15] P.W. Atkins, Physical Chemistry, Oxford Univ. Press, Oxford, 1997.
[16] N. Lopez, J.K. Nørskov, J. Am. Chem. Soc. 124 (2002) 11262.
[17] M. Haruta, Catal. Today 36 (2003) 153.
[18] M. Valden, X. Lai, D.W. Goodman, Science 281 (1998) 1647.
[19] C.T. Campbell, J. Catal. 204 (2001) 520.
[20] J.A. Dumesic, J. Catal. 185 (1999) 496.
[21] J.A. Dumesic, J. Catal. 204 (2001) 525.
[22] T. de Donder, L'Affinité, Gauthier–Villers, Paris, 1927.
[23] R.A. van Santen, J.W. Niemantsverdriet, Chemical Kinetics and Catalysis, Plenum, New York, 1995.
[24] A. Logadottir, J.K. Nørskov, J. Catal. 220 (2003) 273.
[25] H.S. Bengaard, J.K. Nørskov, J.S. Sehested, B.S. Clausen, L.P. Nielsen, A. Molenbroek, J.R. Rostrup-Nielsen, J. Catal. 209 (2002) 365.
[26] B. Hammer, J. Catal. 199 (2001) 171.
[27] P. Sabatier, Ber. Deutsch. Chem. Gesellshaft 44 (1911) 1984.
[28] B. Hammer, L.B. Hansen, J.K. Nørskov, Phys. Rev. B 46 (1999) 7413.
[29] M.C. Payne, M.P. Teter, D.C. Allan, T.A. Arias, J.D. Joannopoulos, Rev. Mod. Phys. 64 (1992) 1045.
[30] G. Kresse, J. Furtmüller, Comp. Mater. Sci. 6 (1996) 15.
[31] D. Vanderbilt, Phys. Rev. B 41 (1990) 7892.
[32] L. Bengtsson, Phys. Rev. B 59 (1999) 12301.
[33] H.J. Monkhorst, J.D. Pack, Phys. Rev. B 13 (1976) 5188.
[34] L.M. Aparicio, J. Catal. 165 (1997) 262.
[35] G.P. van der Laan, A.A.C.M. Beenackers, Catal. Rev.-Sci. Eng. 41 (1999) 255.
[36] K. Aika, A. Ozaki, Catal. Sci. Technol. 1 (1981) 87.
[37] B.E. Niewenhuys, Surf. Rev. Lett. 3 (1996) 1869.
[38] M. Fassihi, V.P. Zhdanov, M. Rinnemo, K.E. Keck, B. Kasemo, J. Catal. 141 (1993) 438.
[39] M. Mavrikakis, M. Bäumer, H.J. Freund, J.K. Nørskov, Catal. Lett. 81 (2002) 153.
[40] S.H. Oh, G.B. Fisher, J.E. Carpenter, D.W. Goodman, J. Catal. 100 (1986) 360.
[41] M.J.P. Hopstaken, J.W. Niemantsverdriet, J. Phys. Chem. B 104 (2000) 3058.
[42] V.P. Zhdanov, B. Kasemo, Surf. Sci. Rep. 29 (1997) 31.
[43] B. Hammer, Phys. Rev. B 63 (2001) 205423.
[44] S. Dahl, A. Logadottir, C.J.H. Jacobsen, J.K. Nørskov, Appl. Catal. A 222 (2001) 19.